THE ASTROPHYSICAL JOURNAL, 348:434–447, 1990 January 10

WARM GAS AND SPATIAL VARIATIONS OF MOLECULAR EXCITATION IN THE NUCLEAR REGION OF IC 342

A. ECKART,[1] D. DOWNES,[2] R. GENZEL,[1] A. I. HARRIS,[1] D. T. JAFFE,[3] AND W. WILD[1]
Received 1988 December 28; accepted 1989 July 11

ABSTRACT

We present maps of the $J = 1 \rightarrow 0$ and $2 \rightarrow 1$ lines of ^{12}CO, ^{13}CO, and $C^{18}O$ in the nuclear region of the galaxy IC 342. We find that the ^{13}CO and $C^{18}O$ $J = 2 \rightarrow 1$ to $J = 1 \rightarrow 0$ line ratios provide the most significant constraints on the physical conditions of the molecular interstellar medium. The observations taken with the IRAM 30 m telescope show that molecular gas in the nucleus sampled by the ^{12}CO line is warm and that physical conditions vary with position in the galaxy. If all isotopic CO line emission originates from the same material, the molecular gas in the central 1 kpc region of IC 342 has a kinetic temperature of ≥ 20 K and a molecular hydrogen density of $\sim 3 \times 10^3$ cm^{-3}. At distances ≥ 500 pc from the center, the kinetic temperature is significantly lower (between 10 K and 20 K). Along a ridge 500 pc east of the center, there may be CO emission from optically thin gas at a temperature of ≥ 40 K. Alternatively the ^{12}CO line emission originates in a small amount of warm gas associated with photodissociation regions and/or a warm interclump medium in star-forming regions. In this case, the ^{13}CO and $C^{18}O$ emission measures the bulk of cold (~ 15 K) and dense ($\sim 10^4$ cm^{-3}) gas in molecular clumps. New far-infrared measurements of the [O I] 63 μm fine-structure line indicate that the atomic and molecular gas pressures are both a few times 10^5 cm^{-3} K, 10 times larger than in our Galaxy.

Subject headings: galaxies: individual (IC 342) — galaxies: interstellar matter — galaxies: nuclei

I. INTRODUCTION

IC 342 is a nearby, face-on Sc galaxy at a distance of 4.5 Mpc with strong $^{12}CO(1 \rightarrow 0)$ emission (Morris and Lo 1978; Rickard and Palmer 1981; Young and Scoville 1982; Lo *et al.* 1984). The $^{12}CO(2 \rightarrow 1)$ emission in a 30″ region centered on the nucleus is optically thick (Knapp *et al.* 1980). The $^{12}CO(1 \rightarrow 0)$ and $(2 \rightarrow 1)$ lines are strongest in the nuclear region, which also emits radio continuum (Turner and Ho 1983) and strong infrared radiation. The 3–1000 μm luminosity of the inner 700 pc is $4 \times 10^9 L_\odot$ (Becklin *et al.* 1980), indicating active star formation. Interferometric $^{12}CO(1 \rightarrow 0)$ observations of the central area reveal a barlike structure. Lo *et al.* (1984) suggest that the gravitational potential of the bar causes noncircular motions of molecular clouds, leading to an enhanced frequency of cloud collisions and star formation.

In this paper, we present maps of the $J = 1 \rightarrow 0$ and $J = 2 \rightarrow 1$ lines of ^{12}CO, ^{13}CO, and $C^{18}O$, with resolutions of 21″ and 14″, along with the first measurement of the 63 μm [O I] fine-structure line toward the nucleus. These data give new information on the spatial variation of excitation, density, and column density of molecular and atomic material in the nuclear region of IC 342.

II. OBSERVATIONS

a) Millimeter Observations

The millimeter observations were made with the IRAM 30 m telescope in 1987 March and October. Independent maps were made of the nuclear region of IC 342 on both occasions. The maps are in good agreement with each other, and only the more extensive 1987 October data set will be discussed here. We used the IRAM SIS receivers (Blundell *et al.* 1985; Blundell, Carter, and Gundlach 1988) and two filter banks of 256×1 MHz channels to simultaneously observe the $J = 1 \rightarrow 0$ and $J = 2 \rightarrow 1$ lines of the ^{12}CO, ^{13}CO, and $C^{18}O$ isotopes. Table 1 summarizes system parameters at 115 and 230 GHz. The system was calibrated by the chopper wheel method (Kutner and Ulich 1981; Ulich and Haas 1976) and by observations of Mars and the Moon. Pointing was checked on 3C 84 and 1044+71 and confirmed by monitoring the line profile at the near-infrared peak of IC 342 (R.A. = $03^h41^m57^s$, decl. = 67°56′29″[1950]). The pointing at 115 and 230 GHz agreed to within 3″. Table 2 lists integration times, sampling, and spatial extent of the measurements for the various isotopes. Line temperatures are given as Rayleigh-Jeans main-beam brightness temperatures, that is, antenna temperatures corrected for atmospheric transmission and main beam efficiencies.

b) Far-Infrared Spectroscopy

Far-infrared data of the $^3P_1 \rightarrow {}^3P_2$ fine-structure transition of neutral oxygen were taken in 1984 July with the NASA Kuiper Airborne Observatory and the UC Berkeley tandem Fabry–Perot spectrometer (Storey, Watson, and Townes 1980; Lugten 1987). The 63 μm system noise equivalent power (NEP) was 5×10^{-14} W Hz$^{-1/2}$. The 63.1837 μm $^3P_1 \rightarrow {}^3P_2$ transition of [O I] was observed with a 60″ beam (FWHM) at a spectral resolution of 165 km s^{-1}. The integrated [O I] line brightness (3.2×10^{-4} ergs s^{-1} cm^{-2} sr^{-1}) was calibrated relative to the continuum of Orion-KL and is accurate to $\pm 40\%$. For comparison with the [O I] line, we use the observation of the 158 μm $^2P_{3/2} \rightarrow {}^2P_{1/2}$ [C II] line at a resolution of 55″ by Crawford *et al.* (1985), who measured a [C II] line brightness of 4.5×10^{-4} ergs s^{-1} cm^{-2} sr^{-1}.

[1] Max-Planck-Institut für Physik und Astrophysik, Institut für Extraterrestrische Physik.
[2] Institute de Radio Astronomie Millimétrique.
[3] Astronomy Department, University of Texas.

TABLE 1

INSTRUMENTAL PARAMETERS

Frequency (GHz)	Beam Width FWHM	Main Beam Efficiency	Receiver Noise Temperature (K)	Spectral Resolution (km^{-1})
115.....	21″	60%	160 SSB	2.6
230.....	14″	45%	240 SSB	1.3

III. RESULTS

In §§ III*a* and III*b*, we present the observations, distribution, and kinematics of the line emission of the CO isotopes. Section III*c* contains an interpretation of the line ratios in terms of the spatial variation of the molecular excitation. Section III*d* is a discussion of the implications of the far-infrared measurements for the interstellar medium in the nuclear region.

a) The Maps

Figure 1*a* and 1*b* shows sample spectra of the CO isotopes near the center of IC 342 and 20″ south. Table 3 lists the velocity integrated line fluxes and their uncertainties for all maps.

Uncertainties in line fluxes are a combination of calibration uncertainty, baseline fitting uncertainty, and rms noise in the data. The absolute calibration was checked by observations of Orion A (see footnote in § IV*b*) and is probably accurate to within 20%. However, the relative calibration between the 115 GHz and 230 GHz measurements is much better since it is subject to differential errors only, such as receiver stability, beam efficiencies, and atmospheric absorption at both frequencies. Monitoring these quantities and comparing the results obtained in 1987 March and November, we estimate the relative calibration to be better than 10%.

We fitted up to second-order baselines to the data. However, since the lines are narrow (less than 50 km^{-1} FWHM) and strong at the center and even narrower off-center, the baseline uncertainties do not contribute significantly. The uncertainties in Table 3 are derived from the velocity-smoothed, baseline-subtracted spectra, which were used for the total line flux maps and the ratio maps. Listed are the rms errors per velocity bin, multiplied with a constant linewidth of 40 km s^{-1}, and divided by the square root of the number of channels covered by the linewidth. For the $J = 1 \rightarrow 0$ data the uncertainties are all of the order of a few percent. Along the molecular bar the errors for the $J = 2 \rightarrow 1$ data are a few percent, and off the bar they are of the order of 10%.

Figures 2*a* and 2*b* give the integrated intensity maps of the $^{12}CO(1 \rightarrow 0)$ and $^{12}CO(2 \rightarrow 1)$ transitions. The line emission comes mainly from a $\sim 30'' \times \leq 13''$ (FWHM) structure and is elongated NS. The emission is centrally peaked and extended to the NE. We also find underlying extended emission over $> 90''$ (2 kpc) at position angle 25°. All components in the $^{12}CO(1 \rightarrow 0)$ maps are present in the higher resolution $2 \rightarrow 1$ map. Within pointing uncertainties ($\leq 3''$), the positions of the central peaks in both maps coincide with the peak positions of radio continuum and IR maps of the nucleus (Becklin *et al.* 1980). In the $^{12}CO(2 \rightarrow 1)$ map, the underlying emission is less pronounced, and the eastern extension is more prominent than in the $1 \rightarrow 0$ map.

Our $1 \rightarrow 0$ and $2 \rightarrow 1$ maps, at 21″ and 14″ resolution, can be compared with the $1 \rightarrow 0$ Cal Tech interferometer data at 7″ resolution (Lo *et al.* 1984) and the $1 \rightarrow 0$ Nobeyama map (Hayashi *et al.* 1986) at 15″ resolution. These maps show a barlike structure elongated in the same direction as in our maps. The lower contours in our $^{12}CO(1 \rightarrow 0)$ map follow the NS structure in the map by Lo *et al.* (1984). Extended emission south of the nucleus in our and the Nobeyama maps is probably resolved and suppressed by the 65″ primary beam of the interferometer. Our maps are centrally peaked, whereas the other maps show two peaks of similar strength separated by $\sim 15''$. The explanation for the latter discrepancy is not clear, as two emission peaks at that separation should at least be clearly visible on our $^{12}CO(2 \rightarrow 1)$ map. We regard our 30 m maps as reliable, since in particular the independent maps obtained from the 1987 March data also are centrally peaked. Remaining differences in the maps are probably due to the different beams, or to components $\geq 30''$ that are resolved out by the interferometer. The extended emission in all three maps is consistent with the $^{12}CO(1 \rightarrow 0)$ map by Rickard *et al.* (1981), at 65″ resolution, which shows a central component extended NS.

Our maps of the $1 \rightarrow 0$ and $2 \rightarrow 1$ lines of the ^{13}CO isotope (Figs. 3*a* and 3*b*) are also similar to each other. In both cases, an elongated structure bends from the south to the northeast. This structure agrees with the ^{12}CO maps and confirms the eastern extension of the central component.

b) Velocity Field

Figure 4 shows the intensity-weighted velocity field of the $^{12}CO(1 \rightarrow 0)$ emission. As in the results of Lo *et al.* (1984), our measurements indicate that the molecular gas is in rotation about the nucleus. The $^{12}CO(1 \rightarrow 0)$ isovelocity lines are (P.A. $-30°$), not parallel to those obtained from H I measurements (P.A. $-50°$; Rogstad and Shostak 1973) and we find a pronounced velocity gradient across the bar.

TABLE 2

PARAMETERS OF THE MAPPING OF CO ISOTOPES IN IC 342

Isotope	Transition	Integration Time (minutes)	Raster Spacing	Offset Range R.A.	Offset Range Decl.	Comments
^{12}CO.....	$1 \rightarrow 0, 2 \rightarrow 1$	≥ 2	10″	−30″ to +30″	−45″ to +45″	Two rasters offset by 5″ in R.A. and decl.; 102 positions measured. $^{12}CO(2–1)$ map fully sampled. $^{12}CO(1–0)$ map oversampled.
^{13}CO.....	$1 \rightarrow 0, 2 \rightarrow 1$	3	10	−10 to +20	−30 to 20	Single-raster $^{13}CO(1 \rightarrow 0)$ map fully sampled. $^{13}CO(2 \rightarrow 1)$ map undersampled.
$C^{18}O$.....	$1 \rightarrow 0, 2 \rightarrow 1$	≤ 36	...	0	0	Three positions measured.
				0	−10	
				+10	0	

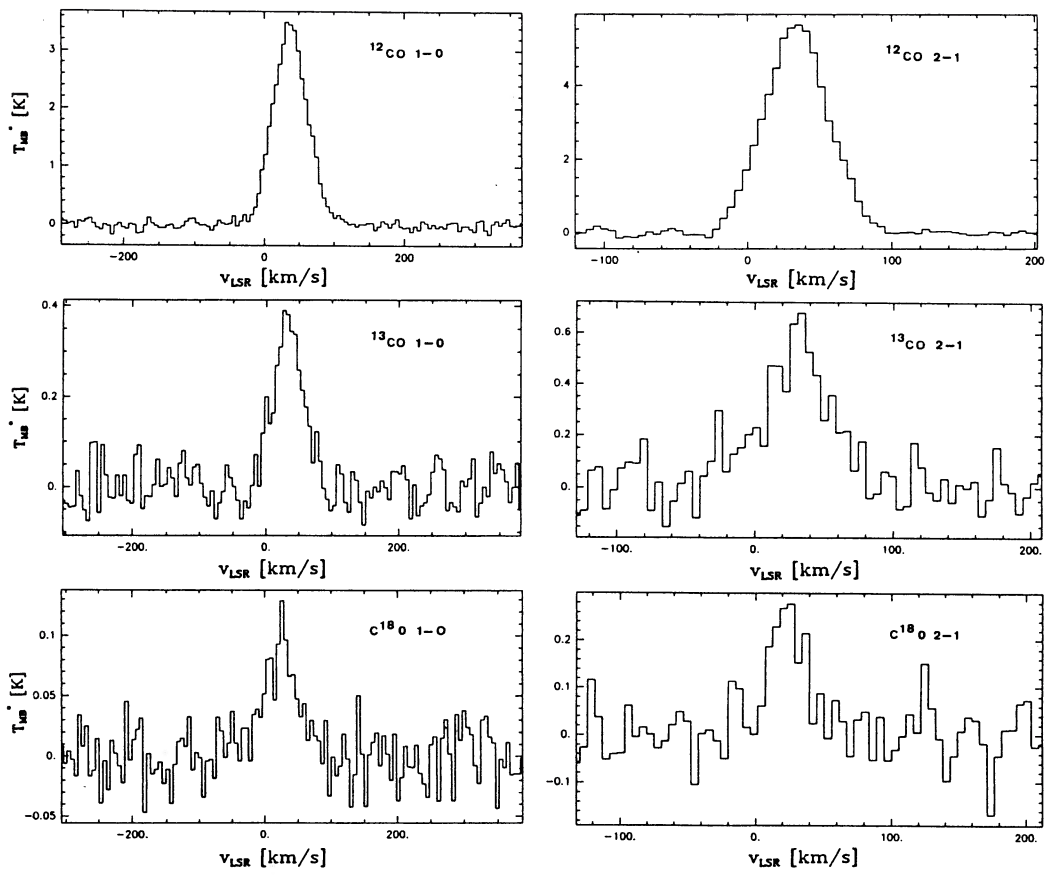

FIG. 1*a*

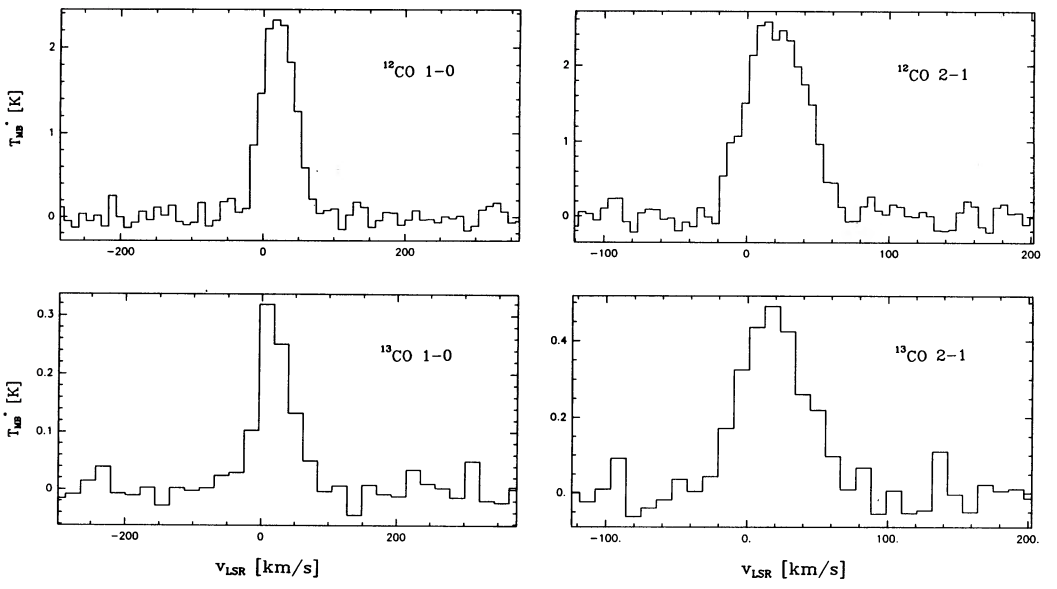

FIG. 1*b*

FIG. 1.—(*a*) Sample spectra for the central position of IC 342. The spectral resolution is 5.2 km s^{-1} and 2.6 km s^{-1} for the $J = 1 \rightarrow 0$ and $2 \rightarrow 1$ lines, respectively. (*b*) Sample spectra for a position 20″ south of IC 342. The spectral resolution is 10.4 km s^{-1} and 2.6 km s^{-1} for the ^{12}CO($1 \rightarrow 0$) and ^{12}CO($2 \rightarrow 1$) lines, respectively. For the ^{13}CO lines, the spectral resolution is 2 times lower.

TABLE 3

LINE FLUXES[a]

Δα	Δδ	$\int T_{mb}\,dv$ (K km s^{-1})	σ	Δα	Δδ	$\int T_{mb}\,dv$ (K km s^{-1})	σ
		^{12}CO(1–0)					
−34″	−45″	9.8	1.3	10″	40″	59.0	1.5
−34	−35	13.3	1.5	10	20	127.0	2.1
−34	−25	23.4	1.7	10	10	139.2	2.3
−34	−15	12.9	1.4	10	0	142.5	1.7
−24	−35	37.7	1.4	10	−10	99.9	2.1
−24	−25	45.3	2.0	10	−20	76.7	1.4
−24	−15	38.9	2.1	10	−30	63.7	1.5
−24	−5	25.3	1.7	10	−40	43.6	1.4
−24	5	26.3	1.7	10	−50	28.3	1.3
−14	−45	46.2	1.9	0	−50	35.8	1.2
−14	−35	63.4	1.4	0	−40	67.8	1.5
−14	−25	90.8	1.8	0	−30	104.5	1.6
−14	−15	113.2	2.1	0	−20	138.7	2.0
−14	−5	96.1	1.6	0	−10	196.7	2.0
−14	5	63.2	1.8	20	−40	28.8	1.7
−14	15	51.5	2.2	20	−30	33.7	1.3
−14	25	45.6	1.5	20	−20	26.9	1.3
−14	35	38.3	1.5	20	−10	27.0	1.2
−4	−55	27.2	1.6	20	0	47.9	1.2
−4	−45	41.3	1.3	20	10	53.2	1.6
−4	−35	87.8	1.2	20	20	53.2	1.6
−4	−25	138.1	1.8	20	30	35.1	1.5
−4	−15	191.0	1.9	20	40	33.2	1.1
−4	−5	205.4	2.1	30	−10	9.9	1.2
−4	5	186.3	1.9	30	0	9.2	1.5
−4	15	128.3	2.1	30	10	22.2	1.6
−4	25	76.5	1.8	30	20	13.3	1.2
−4	35	50.3	1.6	−10	−50	36.3	1.5
−4	45	16.5	1.4	−10	−40	59.4	1.3
−4	55	25.4	1.5	−10	−30	80.8	1.4
6	−45	40.5	1.2	−10	−20	129.6	1.3
6	−35	65.7	1.4	−10	−10	134.5	1.7
6	−25	76.6	1.2	−10	0	128.4	1.7
6	−15	123.4	1.6	−10	10	95.3	1.8
6	−5	168.7	1.7	−10	20	73.0	1.7
6	5	187.5	1.9	−10	30	33.0	1.6
6	15	141.4	2.0	−10	40	33.4	1.3
6	25	82.1	1.8	−20	−50	26.8	1.6
6	35	48.4	1.8	−20	−40	48.8	1.5
16	−55	27.8	1.2	−20	−30	52.0	1.4
16	−45	24.7	1.4	−20	−20	59.1	1.7
16	−35	45.2	1.5	−20	−10	53.5	1.4
16	−25	51.5	1.5	−20	0	36.8	1.6
16	−15	48.5	1.6	−20	10	24.3	1.5
16	−5	58.3	1.8	−20	20	33.7	1.3
16	5	81.7	1.1	−30	−40	10.9	1.2
16	15	71.6	2.1	−30	−30	13.1	1.6
0	10	177.2	1.8	−30	−20	22.3	1.6
0	20	129.6	1.6	−30	−10	19.6	1.9
0	30	70.4	1.4	10	30	68.1	1.1
0	40	46.9	1.8	0	0	213.2	2.1

TABLE 3—*Continued*

Δα	Δδ	$\int T_{mb}\,dv$ (K km s^{-1})	σ	Δα	Δδ	$\int T_{mb}\,dv$ (K km s^{-1})	σ
		^{12}CO(2–1)					
−34″	−45″	19.0	2.4	10″	40″	53.5	1.8
−34	−35	8.0	2.0	10	20	155.6	2.3
−34	−25	−2.0	3.0	10	10	211.3	3.0
−34	−15	10.2	1.9	10	0	202.9	2.0
−24	−35	38.6	2.1	10	−10	105.3	1.7
−24	−25	20.1	2.0	10	−20	53.5	1.5
−24	−15	26.3	1.8	10	−30	51.5	2.2
−24	−5	41.4	2.4	10	−40	48.1	1.2
−24	5	13.5	1.3	10	−50	32.1	1.9
−14	−45	48.3	1.9	0	−50	20.8	1.2
−14	−35	46.2	2.0	0	−40	38.4	1.6
−14	−25	84.3	2.3	0	−30	102.9	1.7
−14	−15	112.8	1.7	0	−20	134.4	2.0
−14	−5	71.7	2.6	0	−10	230.9	2.4
−14	5	82.3	2.5	20	−40	33.4	1.7
−14	15	63.7	1.8	20	−30	28.8	1.7
−14	25	72.1	2.2	20	−20	28.9	1.5
−14	35	56.2	2.3	20	−10	21.2	1.5
−4	−55	16.1	2.5	20	0	14.2	1.3
−4	−45	45.7	2.4	20	10	40.8	1.7
−4	−35	55.0	2.1	20	20	43.2	2.5
−4	−25	129.7	1.8	20	30	44.4	1.9
−4	−15	207.1	2.1	20	40	37.7	2.0
−4	−5	282.2	2.8	30	−10	15.9	1.5
−4	5	226.2	2.3	30	0	15.5	1.6
−4	15	167.3	1.7	30	10	21.7	1.5
−4	25	78.6	2.1	30	20	16.6	2.0
−4	35	44.7	2.1	−10	−50	40.6	2.3
−4	45	26.8	1.8	−10	−40	50.2	2.2
−4	55	1.3	2.1	−10	−30	56.9	1.9
6	−45	24.3	2.0	−10	−20	124.5	3.1
6	−35	53.0	1.6	−10	−10	132.3	2.0
6	−25	60.7	1.2	−10	0	132.7	1.6
6	−15	117.2	1.8	−10	10	62.3	2.2
6	−5	184.9	1.9	−10	20	74.6	2.2
6	5	217.5	2.2	−10	30	27.0	1.7
6	15	136.7	1.7	−10	40	38.1	1.2
6	25	61.4	2.4	−20	−50	16.3	2.0
6	35	52.3	2.1	−20	−40	42.1	1.6
16	−55	8.3	2.2	−20	−30	23.7	1.8
16	−45	24.7	2.2	−20	−20	23.6	1.5
16	−35	27.3	2.2	−20	−10	9.2	1.7
16	−25	21.9	2.7	−20	0	26.2	2.5
16	−15	29.2	2.0	−20	10	20.8	1.6
16	−5	48.7	1.9	−20	20	14.6	1.9
16	5	53.0	1.0	−30	−40	24.2	1.8
16	15	59.6	2.7	−30	−30	−2.0	3.0
0	10	234.2	2.3	−30	−20	10.5	1.7
0	20	167.5	1.7	−30	−10	−2.0	3.0
0	30	33.9	2.2	10	30	56.4	1.3
0	40	36.9	2.0	0	0	324.3	3.2

TABLE 3—*Continued*

$\Delta\alpha$	$\Delta\delta$	$\int T_{mb}\,dv$ (K km s^{-1})	σ	$\Delta\alpha$	$\Delta\delta$	$\int T_{mb}\,dv$ (K km s^{-1})	σ
			^{13}CO(1–0)				
0″	10″	14.9	0.5	−10″	20″	4.8	0.7
0	20	7.1	0.4	20	−10	7.5	0.5
0	−20	18.9	0.4	20	0	10.0	0.5
10	−20	13.6	0.6	20	10	7.9	0.6
10	−10	15.3	0.5	0	−30	10.2	0.7
10	0	19.1	0.4	10	−30	7.1	0.7
10	10	15.6	0.7	−10	−20	14.5	0.5
10	20	8.2	0.6	0	0	18.9	0.5
−10	−10	11.0	0.5	0	−10	18.8	0.4
−10	10	5.8	0.6	−10	0	9.0	0.5
			^{13}CO(2–1)				
0	10	2.6	1.1	−10	10	0.4	1.4
0	20	11.0	1.0	−10	20	−2.0	3.0
0	−20	27.2	1.0	20	−10	12.7	1.2
10	−20	7.1	1.3	20	0	3.2	1.3
10	−10	7.9	1.2	20	10	3.6	0.9
10	0	30.3	1.2	0	−30	7.1	1.1
10	10	21.1	0.7	10	−30	−1.7	2.6
10	20	16.8	1.3	0	0	29.7	1.1
−10	−20	0.2	1.1	0	−10	37.3	0.8
−10	−10	8.0	1.3	−10	0	−0.2	0.3
		C^{18}O(1–0)				C^{18}O(2–1)	
0	0	4.9	0.5	0	0	8.4	1.7

[a] Listed are offsets $\Delta\alpha$, $\Delta\delta$ from the central position in R.A. and decl. in arcseconds, velocity-integrated line fluxes and their uncertainties σ in K km s^{-1} as determined from the spectra used for the maps presented (see text).

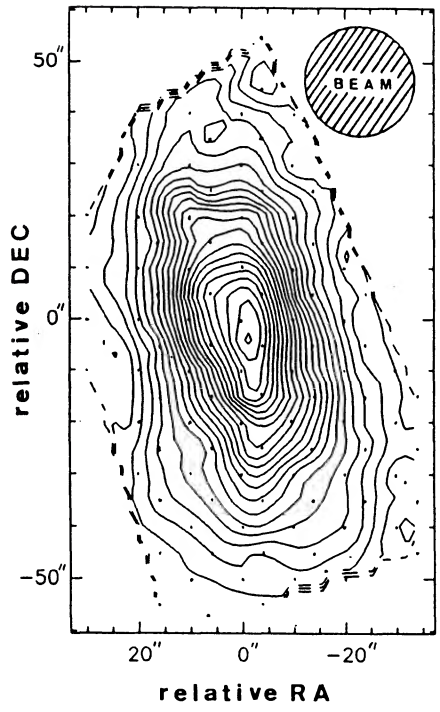

FIG. 2*a*

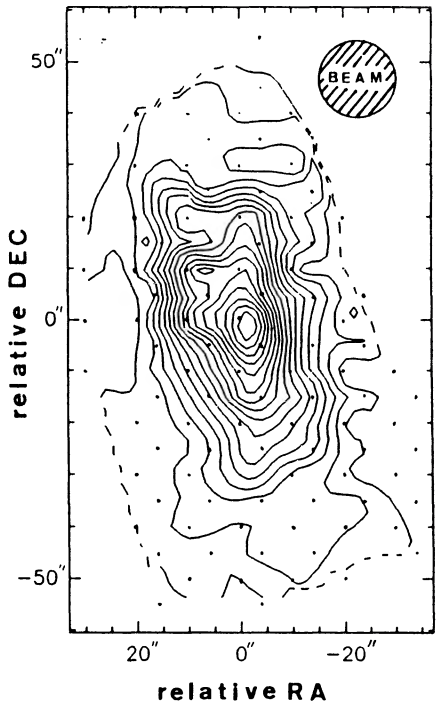

FIG. 2*b*

FIG. 2.—(*a*) Map of ^{12}CO(1 → 0) integrated intensities in IC 342. Contour interval = 10 K, peak = 213 K km s^{-1}. (*b*) Map of ^{12}CO(2 → 1) integrated intensities in IC 342. Contour interval = 20 K km s^{-1}, peak = 324 K km s^{-1}. The base position (0, 0) is R.A. = 03^{h}41^{m}57^s, decl. = 67°56′29″(1950). Dots mark the positions where measurements were taken. The FWHM beam size is indicated in the upper right.

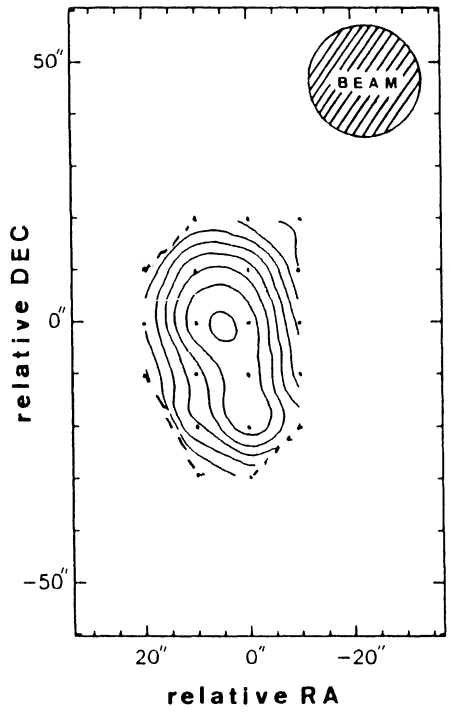

FIG. 3a

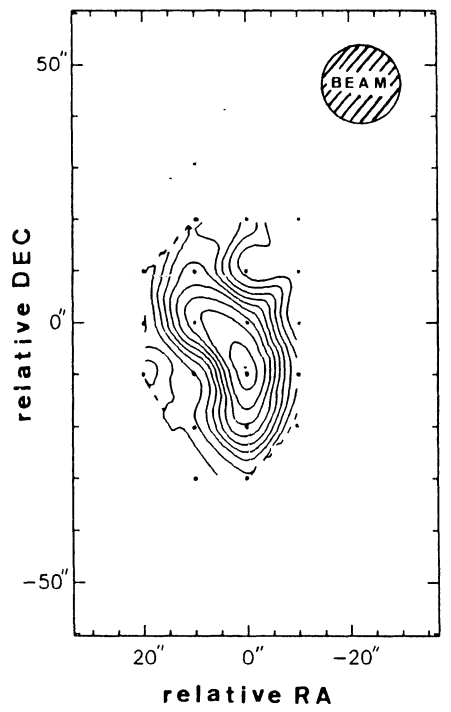

FIG. 3b

FIG. 3.—(*a*) Map of $^{13}CO(1 \rightarrow 0)$ integrated intensities in IC 342. Contour interval = 2 K km s^{-1}, peak = 18.9 K km s^{-1}. (*b*) Map of $^{13}CO(2 \rightarrow 1)$ integrated intensities in IC 342. Contour interval = 4 K km s^{-1}, peak = 37.3 K km s^{-1}. Same base position as in Fig. 2. Dots mark the positions where measurements were taken. The FWHM beam size is indicated in the upper right.

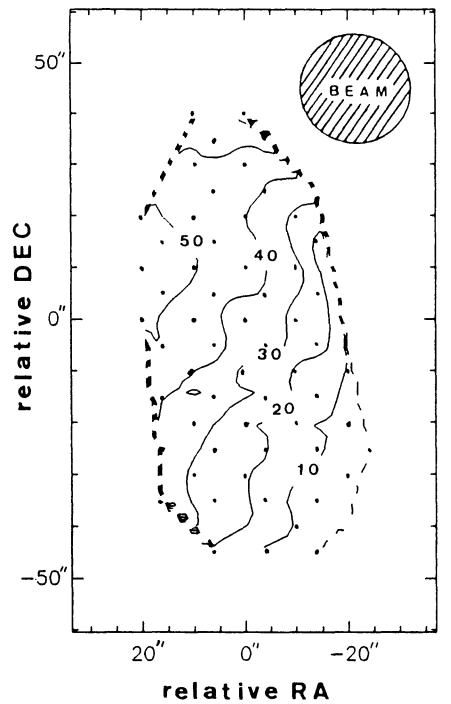

FIG. 4.—Intensity-weighted velocity field of the $^{12}CO(1 \rightarrow 0)$ emission. Velocities are given in intervals of 10 km s^{-1}. Same base position as in Fig. 2. Dots mark the positions where measurements were taken. The FWHM beam size is indicated in the upper right.

The LSR velocity centroids range from <5 km s^{-1} in the SW to >50 km s^{-1} in the NE, with a value of 30 km s^{-1} at the center. Along P.A. 25°, the velocity gradient is 1.5 km s^{-1} arcsec^{-1} in the interferometer map and 0.8 km s^{-1} arcsec^{-1} in our map. As expected for our larger beam, we find a smaller velocity gradient across the central position than do Lo *et al.* (1984).

Maps of $^{12}CO(2 \rightarrow 1)$ emission in various velocity ranges (Fig. 5) show that the central elliptical or bar structure is most prominent in the range $0 < v_{lsr} < 70$ km s^{-1}, with shape, size, and position angle similar to that reported by Lo *et al.* (1984). We also find components with velocities from -40 to $+100$ km s^{-1} (Lo *et al.* did not cover this entire velocity range), along a position angle of 25°, the same as that of the dust lanes NE and SW of the nuclear bulge. The strongest of these components has a velocity centroid of 50 km s^{-1} and is located 10″ NE of the nucleus.

c) Line Ratio Maps

Our aim was to observe two rotational transitions for each of the three CO isotopes, to investigate the physical conditions of the molecular gas. Since the source is small, the main beam efficiencies are large (see Table 1), and the $J = 2 \rightarrow 1$ and $1 \rightarrow 0$ data were obtained simultaneously, accurate ratios can be derived (see also discussion of uncertainties in § III*a*). Below we show that the most interesting new finding is that the $2 \rightarrow 1$ to $1 \rightarrow 0$ ^{13}CO and $C^{18}O$ line ratios near the nucleus only slightly exceed unity, and definitely do not approach 4, the ratio for optically thin, high-temperature gas.

Maps of the line ratios shown in Figure 6 were obtained in the following way. We first convolved the $^{12}CO(2 \rightarrow 1)$ and $^{13}CO(2 \rightarrow 1)$ maps with a Gaussian to the resolution of the

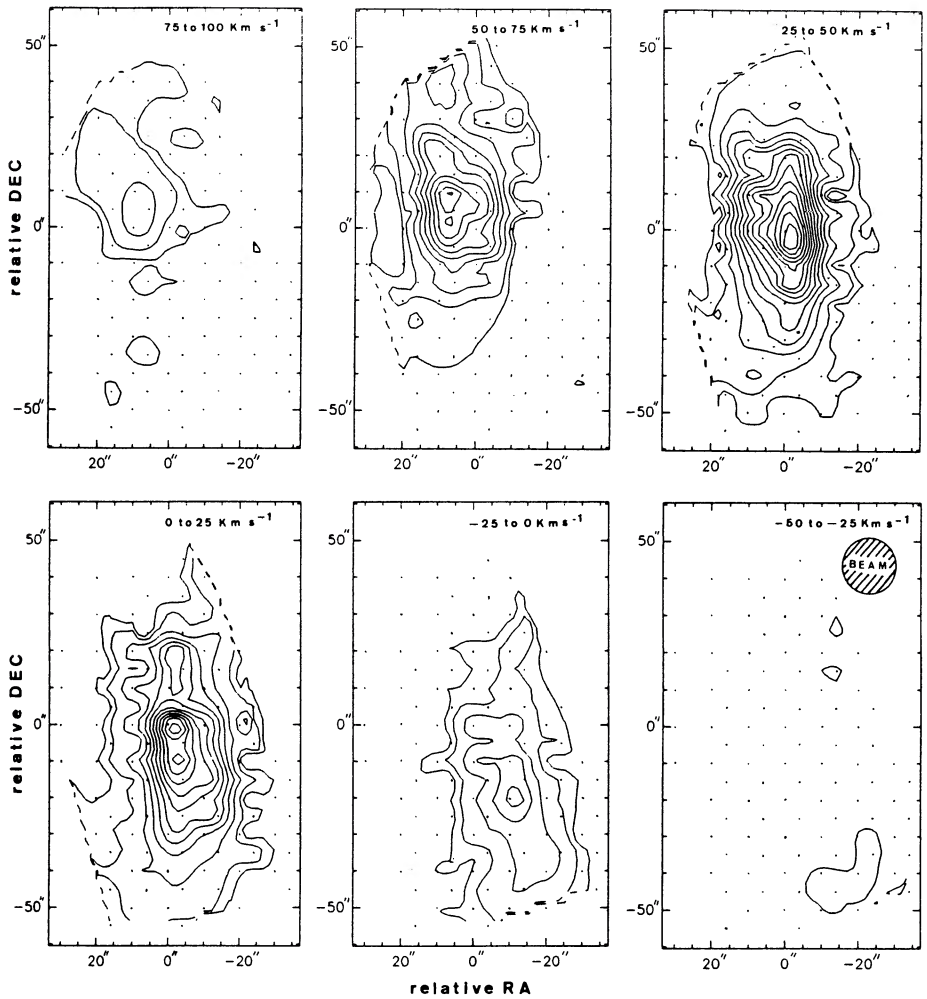

FIG. 5.—Channel maps of the $^{12}CO(2 \rightarrow 1)$ emission. Contour levels are 5, 10, 20 ... K km s^{-1}. In each map, the upper and lower velocity bounds are given in km s^{-1}. Same base position as in Fig. 2. Dots mark the positions where measurements were taken. The FWHM beam size is indicated in upper right of the lower right panel.

corresponding $J = 1 \rightarrow 0$ maps, in order to correct for the different beamwidths at 115 and 230 GHz. As a second method, we also deconvolved the oversampled $^{12}CO(1 \rightarrow 0)$ map with a maximum entropy algorithm, and then reconvolved it with the 14″ beam of the $2 \rightarrow 1$ measurements (Fig. 7). The convolution method is less sensitive to local variations and gives a more reliable picture of extended emission. The second procedure yields maps with a higher angular resolution, but depends more critically on the pointing, data quality, beam shape, etc. Judging from the uncertainties of the line fluxes given in Table 3 (see also § III*a*) as well as from a comparison to our independent data from 1987 March, the uncertainties in the line ratio maps in Figures 6*a* and 6*c* for which we used the convolved $J = 2$–1 maps are of the order of 10%. Uncertainties in the line ratio map shown in Figure 6*b* are of the order of 15%. We consider features to be real if they are in both of the reduced maps.

In the following we briefly discuss how the physical conditions can be derived from the data and what the basic conclusions are for the nucleus of IC 342. For sources convolved to the same resolution, we can approximate the $J = 2 \rightarrow 1$ to $1 \rightarrow 0$ line temperature ratio by

$$\frac{T_{21}^{mb}}{T_{10}^{mb}} = \frac{(1 - e^{-\tau_{21}})\,(T_{21} - T_{21}^{bg})}{(1 - e^{-\tau_{10}})\,(T_{10} - T_{10}^{bg})} \quad (1)$$

where the subscripts 21, 10 refer to the $2 \rightarrow 1$ and $1 \rightarrow 0$ lines. T^{mb} is the main beam brightness temperature, τ the opacity, and T the equivalent Rayleigh-Jeans excitation temperature, which is related to the true excitation temperatures, T_{ex}, by

$$T = (h\nu/k)[\exp\,(h\nu/kT_{ex}) - 1]^{-1}\,. \quad (2)$$

Similarly, T^{bg} is the equivalent Rayleigh-Jeans temperature of the 2.75 K cosmic background at the frequency of the relevant transition. At 230 GHz, $T^{bg} = 0.20$ K, and at 115 GHz, $T^{bg} = 0.85$ K. For optically thick ($\tau \gg 1$) ^{12}CO gas,

$$\frac{T_{21}^{mb}}{T_{10}^{mb}} = \frac{T_{21} - T_{21}^{bg}}{T_{10} - T_{10}^{bg}} = \frac{11.03[\exp\,(11.03/T_{ex}) - 1]^{-1} - 0.20}{5.52[\exp\,(5.52/T_{ex}) - 1]^{-1} - 0.85} \quad (3)$$

and in the optically thin case, for $T_{ex} \gg 2.75$ K,

$$\frac{T_{21}^{mb}}{T_{10}^{mb}} = \frac{\tau_{21}(T_{21} - T_{21}^{bg})}{\tau_{10}(T_{10} - T_{10}^{bg})} \approx 4 \exp\left(-\frac{11.03}{T_{ex}}\right). \quad (4)$$

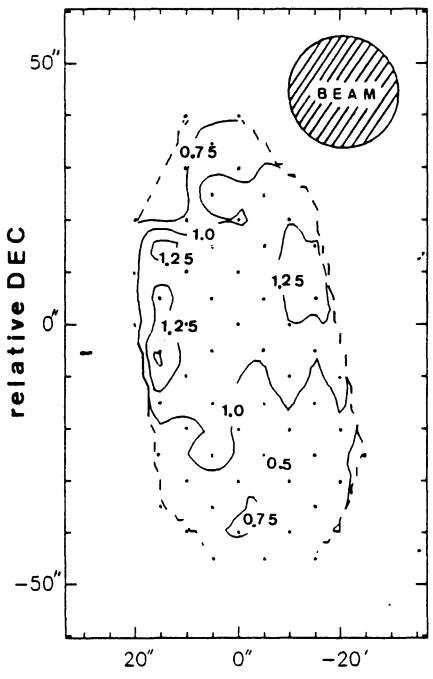

FIG. 6a

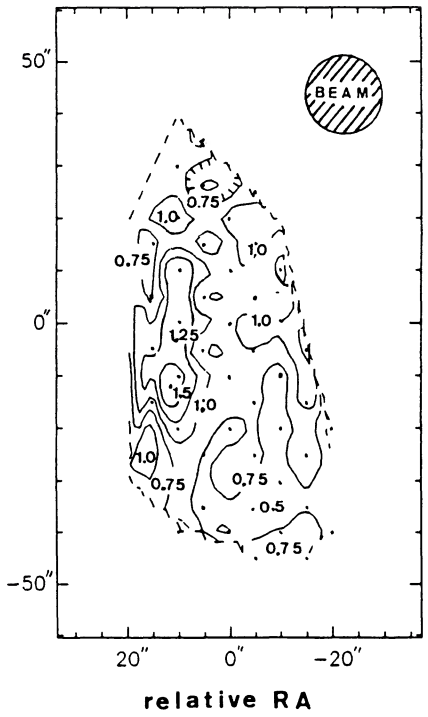

FIG. 6b

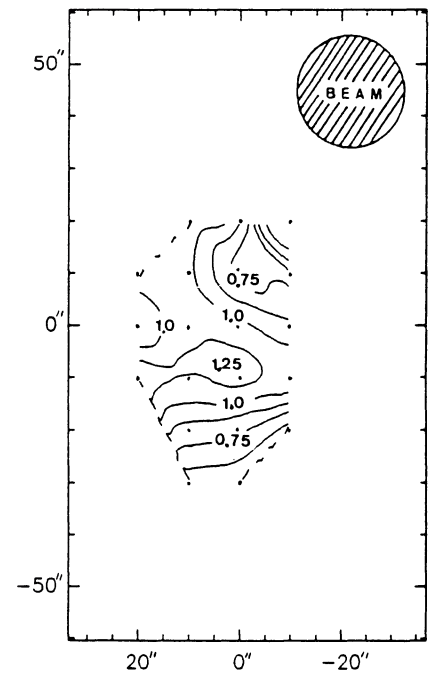

FIG. 6c

FIG. 6.—Ratios of integrated intensities of the $2 \rightarrow 1$ and $1 \rightarrow 0$ lines. (*a*) Ratio of integrated intensities in the $^{12}CO(2 \rightarrow 1)$ and $(1 \rightarrow 0)$ maps. The $2 \rightarrow 1$ map is convolved to the 21″ resolution of the $1 \rightarrow 0$ map. (*b*) Ratio of integrated intensities of the $^{12}CO(2 \rightarrow 1)$ and $(1 \rightarrow 0)$ maps. The $1 \rightarrow 0$ map is deconvolved by a maximum entropy algorithm and then reconvolved to the 14″ resolution of the $2 \rightarrow 1$ map. (*c*) Ratio of integrated intensities of the $^{13}CO(2 \rightarrow 1)$ and the $(1 \rightarrow 0)$ maps. The $2 \rightarrow 1$ map is convolved to the resolution of the $1 \rightarrow 0$ map. Same base position as in Fig. 2. Dots mark the positions where measurements were taken. The FWHM beam size is indicated in the upper right.

Hence, we expect $(2 \rightarrow 1)/(1 \rightarrow 0)$ line temperature ratios near 1.0 for dense, warm, optically thick gas, and 4 for dense, warm and optically thin gas. A ratio <1 can indicate low temperatures for optically thick lines, due to the exponential dependence of the line ratio on excitation temperature, T_{ex}. Deviations from the LTE values for optically thick and thin line emission can also occur when the density is too low to thermally populate the rotational levels, as in many envelopes of clouds in our Galaxy.

The most significant finding is that the $2 \rightarrow 1$ to $1 \rightarrow 0$ ^{13}CO and $C^{18}O$ line ratios near the nucleus only slightly exceed unity, and definitely do not approach 4, the ratio for optically thin, high-temperature gas. Therefore, these ratios significantly constrain the physical properties of the molecular gas. The $C^{18}O$ lines are almost certainly optically thin. Since the ^{12}CO emission comes from warm gas, the low $C^{18}O(2 \rightarrow 1)/(1 \rightarrow 0)$ ratio—and hence the low $^{13}CO(2 \rightarrow 1)/(1 \rightarrow 0)$ ratio as well—indicate that the rotational levels are not thermalized. A first qualitative conclusion from the density sensitive ^{13}CO and $C^{18}O$ line ratios is thus that the average hydrogen density is lower than 2×10^4 cm^{-3}.

The $^{12}CO(2 \rightarrow 1)/(1 \rightarrow 0)$ ratio within 20″ of the center of IC 342 is close to unity (Table 4), consistent with optically thick emission from moderately warm gas. The very conservative lower limit to the line ratio of 0.80 (mean value minus 3 times the uncertainty) corresponds to a lower limit to the gas temperature of 10 K. Along a ridge ~20″ east of the center of the galaxy, the $^{12}CO(2 \rightarrow 1)/(1 \rightarrow 0)$ ratio appears to be greater than unity. The most straightforward, although not unique, interpretation of this finding is that the ^{12}CO emission is from warm, partially optically thin gas. An alternative explanation could be that the molecular clouds are heated externally (Young and Scoville 1984), and that the optically thicker $^{12}CO(2 \rightarrow 1)$ line then samples warmer gas closer to the cloud surfaces. Beyond 20″ N and S of the center, the ratio drops to

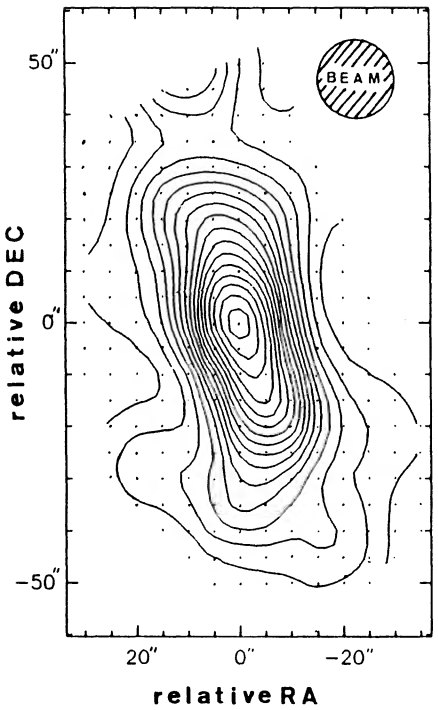

FIG. 7.—Map of $^{12}CO(1 \rightarrow 0)$ integrated intensities deconvolved with a maximum entropy algorithm and then reconvolved to the 14″ resolution of the $^{12}CO(2 \rightarrow 1)$ map. Contour interval = 20 K km s^{-1}, peak = 350 K km s^{-1}. Same base position as in Fig. 2. Dots mark grid positions. The FWHM beam size is indicated in the upper right.

≤ 0.75, indicating lower gas temperatures at greater distances from the nucleus; the average temperature is ≥ 13 K at $R \geq 450$ pc. An interpretation in terms of a radially decreasing gas density and hence, subthermal excitation, is less likely. The ^{12}CO emission is highly opaque, so the corresponding critical H_2 density for thermalization of the ^{12}CO $J = 2$ level (the density where collisional deexcitation and spontaneous radiation rates are equal), is much lower than its value in the optically thin case [$n_{crit}(J = 2) \sim 2 \times 10^4$ cm^{-3}] and, almost certainly lower than the gas density in the source IC 342. The ratio of the $^{13}CO(2 \rightarrow 1)$ to $(1 \rightarrow 0)$ lines mimics the spatial variation of the ^{12}CO ratios.

The observed parameters and our qualitative conclusions are summarized in Table 4 for four regions; the nucleus, the areas 25″N and S of the center, and the ridge 20″ E of the center (hereafter the "eastern ridge"). More quantitative conclusions require a numerical treatment of excitation and radiative transfer. They are discussed in § IV*b*.

d) Atomic Gas

The far-infrared fine-structure lines of [O I] at 63 μm and [C II] at 158 μm arise in the partially ionized medium where hydrogen is mostly neutral and where most molecules are photodissociated. The ratio of the high-excitation [O I] line ($n_{crit} \sim 10^5$–10^6 cm^{-3}) to the lower excitation [C II] line ($n_{crit} \sim 3 \times 10^3$ cm^{-3}) is a measure of the pressure of the warm atomic gas (see discussion in Watson 1982). For a straightforward evaluation of the line ratio, the [O I] and [C II] regions must be coextensive and the line emission must be optically thin. On a global scale, there is good evidence for both assumptions, although the lines are very likely optically thick in special regions (Crawford *et al.* 1985; Stacey 1985; Boreiko, Betz, and Zmuidzinas 1988; Stacey *et al.* 1990). Our analysis follows that by Watson *et al.* (1984), Genzel *et al.* (1985), and Lugten *et al.* (1986).

In IC 342, the [O I] 63 μm to [C II] 158 μm line ratio is 0.8 ± 0.3. In collisionally excited neutral gas [$n_e \leq 10^{-3} n$ (H + H_2)], with an $O^0/C^+ = O/C$ fractional abundance similar to the solar neighborhood (~ 2), this line ratio corresponds to a gas pressure $n_H T \sim 10^6$ cm^{-3} K. For a lower O^0/C^+ ratio, the inferred pressure must be correspondingly higher. For any reasonable gas temperature ($T \leq 500$ K), the inferred hydrogen density of the atomic gas emitting the far-infrared fine structure lines is at least 10^3 cm^{-3}. As in other Galactic and extragalactic sources, we conclude that the [C II]/[O I] emission comes from dense, warm, photodissociated gas at the surfaces of molecular clouds exposed to UV radiation from embedded or external OB stars (Crawford *et al.* 1985; Stacey *et al.* 1985). In several Galactic star-forming regions and the nuclear region of M82, estimates of the mean gas temperature of photodissociation regions are ~ 100–300 K

TABLE 4

MEASURED PARAMETERS AND INTERPRETATION FOR SELECTED AREAS IN IC 342

Position	Quantity	^{12}CO	^{13}CO	$C^{18}O$	Interpretation
Center	$T_{mb}(1 \rightarrow 0)$	8–10 K[a]	0.6–0.9 K[a]	0.25 ± 0.05 K[a]	Emission from
	$I(2 \rightarrow 1)/I(1 \rightarrow 0)$	1.1 ± 0.1	1.0 ± 0.1	1.3 ± 0.3	warm, optically
	$\frac{I[^{12}CO(1 \rightarrow 0)]}{I[\text{isotope}(1 \rightarrow 0)]}$	...	11 ± 4	35 ± 10	thick gas
20″–30″ south and north of center	$T_{mb}(1 \rightarrow 0)$ (K)	2–3[b]	0.25 ± 0.4[b]	...	Emission from
	$I(2 \rightarrow 1)/I(1 \rightarrow 0)$	0.7–0.8	0.5–0.8	...	cold gas at
	$\frac{I[^{12}CO(1 \rightarrow 0)]}{I[^{13}CO(1 \rightarrow 0)]}$	...	11 ± 4	...	$T \geq 13$ K
Eastern ridge	$T_{mb}(1 \rightarrow 0)$ [K]	3–4 K[b]	0.5–0.7 K[b]	...	Emission from warm,
	$I(2 \rightarrow 1)/I(1 \rightarrow 0)$	1.1–1.6	...	...	partially optically
			1.0 ± 0.2	...	thin gas at
	$\frac{I[^{12}CO(1 \rightarrow 0)]}{I[^{13}CO(1 \rightarrow 0)]}$	...	11 ± 4	...	$T > 40$ K

[a] Corrected for component size of 30″ × 13″ (see text).
[b] Corrected for component size of 25″ derived from comparisons of $I(2 \rightarrow 1)/I(1 \rightarrow 0)$ ratios.

(Genzel and Stacey 1985). For a gas temperature of 200 K, we infer a hydrogen density of $\sim 3 \times 10^3$ cm^{-3} and a pressure of 6×10^5 cm^{-3} K for the [C II] and [O I] emitting gas in IC 342. For comparison, Lugten *et al.* (1986) derive a gas pressure of 10^6–10^7 cm^{-3} K for the central kpc of the starburst galaxy M82.

Since the far-infrared fine-structure lines are the dominant coolants of the photodissociated interstellar medium, the far-infrared line-to-continuum ratio measures the efficiency of gas heating by UV radiation. The total far-infrared luminosity of IC 342 is 4×10^9 $L_\odot$ (Becklin *et al.* 1980), while the [C II] luminosity is 2.3×10^7 $L_\odot$, or about 0.5% of the far-infrared continuum luminosity. For comparison, the 158 μm [C II] line in M82 contains $\sim 0.2\%$ of the total far-infrared luminosity of 3×10^{10} $L_\odot$. Hence, the heating efficiencies in both galaxies are comparable, while total far-infrared luminosity and gas pressure in photodissociation regions are more than 10 times lower in IC 342.

As the [C II]/[O I] emission comes from a region where hydrogen is partially atomic (Tielens and Hollenbach 1985), it is interesting to compare hydrogen column densities inferred from the [C II] and 21 cm H I lines. For gas temperatures near 200 K, hydrogen densities of about 3×10^3 cm^{-3}, and from the observed [C II] intensity near the nucleus of IC 342, we calculate a beam-averaged C^+ column density of 4×10^{17} cm^{-2} (Crawford *et al.* 1985). If the [C II] line is optically thin, and if all of the carbon is singly ionized ($C^+/H = 3 \times 10^{-4}$), then the column density of hydrogen nuclei is $N_H^0(C^+) = 1.4 \times 10^{21}$ cm^{-2}. If the abundance is lower than this maximum value or if the line is not optically thin, $N_H^0(C^+)$ is a lower limit to the total hydrogen column density in the [C II] zone.

Observations of the 21 cm H I line in IC 342, with a resolution of 2′ (Rogstad and Shostak 1973) show that the nucleus is at a minimum of the 21 cm emission, with an integrated H I flux ≤ 100 K km s^{-1}. For optically thin gas, this flux corresponds to an atomic hydrogen column density of $N_H = 1.8 \times 10^{20}$ cm^{-2}, or only 10% of N_H^0 (C^+). Hence, the atomic hydrogen column density derived from the 21 cm line is at most 10% of the total column density of hydrogen nuclei in the C^+ zones.

This result is somewhat surprising and probably relevant to the interpretation of 21 cm emission on galactic scales. It indicates that at least a sizable fraction of the 21 cm H I emission may originate in warm, dense, photodissociation regions at the surfaces of molecular clouds (Shaya and Federman 1987). The standard interpretation is that most of the H I emission comes from 80 K "H I clouds" of density $n_H \simeq 10$–100 cm^{-3} (e.g., Kulkarni and Heiles 1988). In reaching our conclusion above, we have taken into account that most of the hydrogen in [C II] regions may be molecular due to H_2 self-shielding (see Jura 1978; Tielens and Hollenbach 1985) and that the H I measurements by Rogstad and Shostak (1973) were taken with a beam twice as large as in the [C II] observations. The same arguments hold for other spiral galaxies with a high rate of star formation (Crawford *et al.* 1985; Stacey *et al.* 1988) and possibly for the global H I emission in our Galaxy (Stacey *et al.* 1985; Stacey 1985).

IV. DISCUSSION

Our new observations demonstrate the value of multiline, multi-isotope measurements for investigating physical conditions in the molecular medium in galaxies. A first qualitative inspection of the data indicates that the molecular gas temperature in the central few hundred pc of IC 342 is significantly higher than in the disk region in IC 342 and in our Galaxy. We now discuss our more detailed model of the CO excitation and radiative transfer.

a) Model Calculations of CO Excitation and Radiative Transfer

In the following, we present simple "one-component" models of the molecular gas, which assume that the emission of ^{12}CO, ^{13}CO, and C^{18}O isotopes all arise in regions with similar physical conditions. In an alternative "two-component" model the ^{12}CO emission would originate from a small amount of warm, low-density molecular gas in photodissociation regions and/or a warm interclump medium in star-forming regions. The bulk of the molecular material will not be influenced by this small amount of warm gas and the ^{13}CO and C^{18}O emission then measures the large amount of cold (~ 15 K) and dense ($\sim 10^4$ cm^{-3}) molecular gas contained in the clumps.

For the "one-component" the ratios of ^{12}CO ($2 \rightarrow 1$) to ($1 \rightarrow 0$) or ^{13}CO and C^{18}O ($2 \rightarrow 1$) to ($1 \rightarrow 0$) can be used simultaneously to constrain the physical parameters. These models follow Martin, Sanders, and Hills (1984) and take into account varying filling factor due to different optical depths in different rotational transitions. They are valid for internally as well as externally heated molecular clouds, but do not take into account temperature gradients. For more quantitative results, we therefore calculated simple models of CO excitation and radiative transfer, as follows.

1. First, the local molecular excitation in an individual molecular clump was calculated from rate equations in an escape probability, radiative transfer formalism (Genzel *et al.* 1989). We computed populations of the 10 lowest rotational levels of ^{12}CO, ^{13}CO, and C^{18}O as functions of hydrogen density, CO column density and kinetic temperatures from 7 to 100 K, with cross sections for collisions of CO with H_2 from Flower and Launay (1985), Schinke *et al.* (1985), and McKee *et al.* (1982). We assumed statistical equilibrium, and fractional abundances $^{12}CO/H_2 = 8 \times 10^{-5}$, $^{12}CO/^{13}CO = 60$, and $^{12}CO/C^{18}O = 500$. Since observations of molecular clouds near our own Galactic center suggest an enhancement of rare CO isotopes, we calculated a second grid with $^{12}CO/^{13}CO = 30$ and $^{12}CO/C^{18}O = 300$. We assumed the local line width in a given clump, $\Delta v_{\rm local} = 5$ km s^{-1} FWHM.

2. Molecular clouds in our Galaxy are clumpy, and the large-scale filling factor and spectral profiles depend on the opacities of the various CO transitions and isotopes. Our model follows Martin, Sanders, and Hills (1984), letting each clump have a velocity width $\Delta v_{\rm local}$, while the ensemble has a macroturbulent velocity width $\Delta v_{\rm cloud}$. In our calculations, we assumed $\Delta v_{\rm cloud}/\Delta v_{\rm local} = 2.5$, and an area filling factor per velocity interval $F_0 = 0.5$, typical of molecular clouds in our Galaxy. We also followed Martin, Sanders, and Hills (1984) in deriving the area filling factor for a given opacity by assuming Gaussian density profiles for individual clumps and then calculating the resulting line profiles. The inputs to the "clumpy cloud" model are the excitation temperature and opacities of the different CO lines calculated in step 1. At a distance of 4.5 Mpc, a beam size of 14″ corresponds to 300 pc, a scale 4–8 times larger than giant molecular clouds in our own Galaxy. Hence, a final parameter is the "global" filling factor, Ψ_0, of clouds per velocity interval per beam. This parameter is computed by comparing the predicted flux of an optically thin line

from step 2) to the observed flux, since an optically thin line gives the total number of molecules in the beam, whatever the gas distribution. In the computation of line-averaged column density we multiplied clump column densities by $\Delta v_{\rm total}/\Delta v_{\rm cloud}$, $\Delta v_{\rm total}$ being the observed line width.

This modeling is probably the simplest approach, taking into account non–LTE, clumpiness and opacity-dependent filling factors. Its principal shortcoming is that the calculations are neither fully self-consistent nor completely physical. Radiative interaction between different clumps at the same velocity is neglected in calculating molecular excitation. Since the excitation calculations in step 1 assume spatially constant density (and excitation temperature), the Gaussian "clump density" profile in step 2 must be interpreted as a profile of column density (this shortcoming has only a minor effect for optically thick ^{12}CO and optically thin C^{18}O lines). Furthermore, there is in reality a range of densities and temperatures in the gas. The model thus gives only a first-order, average picture. The resulting "best physical parameters" of our modeling are listed in Table 5. Figure 8 shows how the observables in Table 4 constrain the model. The main results are as follows:

1. At the central position, the temperature is 20 K or greater, and the pressure of the molecular gas is $\geq 6 \times 10^4$ K cm^{-3}. For a molecular abundance of $[^{12}\mathrm{CO}]/[^{13}\mathrm{CO}] = 30$, the required H_2 density is $\sim 2 \times 10^3$ cm^{-3}.

2. At the eastern ridge, the temperature is ≥ 40 K and the H_2 density is lower ($\sim 10^3$ cm^{-3}). The pressure of the molecular gas is $\geq 4 \times 10^4$ K cm^{-3}. The ^{12}CO emission is partially optically thin ($\tau \sim$ is a few; but see comments in § III*c*).

3. 500 pc N and S of the nucleus, the molecular gas is cooler ($10\ \mathrm{K} \leq T_{\rm kin} \leq 20\ \mathrm{K}$), H_2 densities are a few 10^3 cm^{-3}, and the gas pressure is > a few 10^4 K cm^{-3}.

4. Excepting the eastern region the $^{12}\mathrm{CO}(1 \rightarrow 0)$ optical depths of the individual clumps in the molecular bar are 10–25. We find optical depths ranging from 0.15 to 0.5 for ^{13}CO and 0.02 to 0.1 for C^{18}O.

For the nucleus, the derived kinetic temperature of 20 K or greater is reasonably consistent with the gas kinetic temperature of ~ 70 K derived by Ho, Turner, and Martin (1987) from 1.2 cm inversion lines of NH_3. The presence of radiation from dense and warm molecular gas is also in agreement with recent measurements of the $^{12}\mathrm{CO}(3\text{–}2)$ emission from the nucleus of IC 342 (Ho and Martin 1986; W. Wall, private communication). At the center, the pressures of the atomic and molecular gas are comparable, $\sim 10^5$ K cm^{-3}. This finding is consistent with the picture (Crawford *et al.* 1985) that far-infrared and millimeter CO emission originate in the same, or at least adjacent, regions, such as the photodissociation regions at the surfaces of molecular clouds.

b) H_2 *Mass*

At the individual positions, the ^{12}CO column densities, combined with the assumed fractional abundance $[^{12}\mathrm{CO}]/[\mathrm{H_2}]$ of 8×10^{-5}, the integrated $^{12}\mathrm{CO}(1 \rightarrow 0)$ line intensities, and our "global" filling factor Ψ_0, yield conversion factors $N(\mathrm{H_2})/I[^{12}\mathrm{CO}(1 \rightarrow 0)]$. In the central region of IC 342, our model calculations result in conversion factors surprisingly close to the value of 3–4 $\times 10^{20}$ cm^{-2}/K km s^{-1} (Solomon *et al.* 1987) derived for molecular clouds in the Galaxy.[1] While the amount of molecular gas derived from our results for the central position agrees with the standard conversion factor, it differs by a factor of 2 at the eastern ridge and the positions N and S of the nucleus. Integrating over the ^{12}CO map, and applying the standard conversion factor of 4×10^{20} cm^{-2}/K km s^{-1}, we derive a total molecular mass of $2 \times 10^8\ M_\odot$ contained in the cental 2.5 kpc^2 of IC 342, which agrees with the value of $2.4 \times 10^8\ M_\odot$ in a 65″ single-dish beam obtained by Lo *et al.* (1984). For the ^{13}CO isotope at the three representative positions, we derive a conversion factor $N(\mathrm{H_2})/I(^{13}\mathrm{CO}) \approx 4 \times 10^{21}$ cm^{-2}/K km s^{-1}. Integrating over the $^{13}\mathrm{CO}(1 \rightarrow 0)$ map and applying this conversion factor, we find a molecular mass $\sim 1.5 \times 10^8\ M_\odot$ in the central 1.5 kpc^2.

c) *What Heats the Molecular Gas?*

i) *Dust*

Becklin *et al.* (1980) find a dust temperature of 42 K for the central arcminute of IC 342. For the center, our calculations result in a gas temperature close to the dust temperature. With the moderately high gas densities derived here, dust-gas collisions will be sufficiently effective in cooling the gas temperature to the dust temperature. Hence dust-gas collisions are a likely mechanism for heating the molecular gas. Note, however, that at 42 K the dust cannot explain heating of the bulk of the molecular gas in a single-component model: Calculating the dust mass following Hildebrand (1983) via

$$M_{\rm dust} = \frac{4}{3}\frac{a\rho}{Q_\nu}\frac{S(\nu)D^2}{B(\nu, T_{\rm dust})} \qquad (5)$$

[1] For easy comparison with other data these conversion factors are given on the "Kitt Peak" scale [$T^{\rm mb}_{J=1\rightarrow 0}$(Orion A) = 65 K]; the corresponding conversion factors on the IRAM scale [$T^{\rm mb}_{J=1\rightarrow 0}$(Orion A) = 100 K, Trapezium/Bar] are 0.65 times the Kitt Peak conversion factors. For the ^{12}CO $J = 2 \rightarrow 1$ line we find on the IRAM scale $T^{\rm mb}_{J=2\rightarrow 1}$(Orion A, Trapezium/Bar) = 100 K.

TABLE 5

DERIVED PHYSICAL PARAMETERS FOR SELECTED AREAS IN IC 342

Position	Assumed Abundances $^{12}\mathrm{CO}/\mathrm{H_2}$	$^{12}\mathrm{CO}/^{13}\mathrm{CO}$	$^{12}\mathrm{CO}/\mathrm{C^{18}O}$	$T_{\rm kin}$ (K)	$n_{\rm H_2}$ (cm^{-3})	Pressure $n_{\rm H_2}T$ (cm^{-3} K)	Beam-averaged Column Density $\langle N_{\rm CO}\rangle$ (cm^{-2})	IRAM 30 m Integrated Intensity $I_{^{12}\mathrm{CO}(1-0)}$[a] (K km s^{-1})	Conversion Factor $N_{\rm H_2}/I_{\rm CO}$ on Kitt Peak Scale[a] (cm^{-2}/K km s^{-1})
Center	8×10^{-5}	30	300	≥ 20	2×10^3	4×10^4	3×10^{18}	213	3×10^{20}
Center	8×10^{-5}	60	500	≥ 20	3×10^3	6×10^4	4×10^{18}	213	4×10^{20}
East ridge	8×10^{-5}	60	500	≥ 40	$\sim 10^3$	4×10^4	1.7×10^{18}	140	2.4×10^{20}
25″ N + S	8×10^{-5}	60	500	≥ 13	10^3–10^4	10^4–10^5	$(0.5\text{–}1.5) \times 10^{18}$	110	$(2\text{–}4) \times 10^{20}$

[a] For easy comparison with other data, these conversion factors are given on the "Kitt Peak" scale [$T_{J=1\rightarrow 0}$ (Orion A) = 65 K]; the corresponding conversion factors on the IRAM scale [$T_{J=1\rightarrow 0}$(Orion A] = 100 K are 0.65 times the Kitt Peak conversion factors.

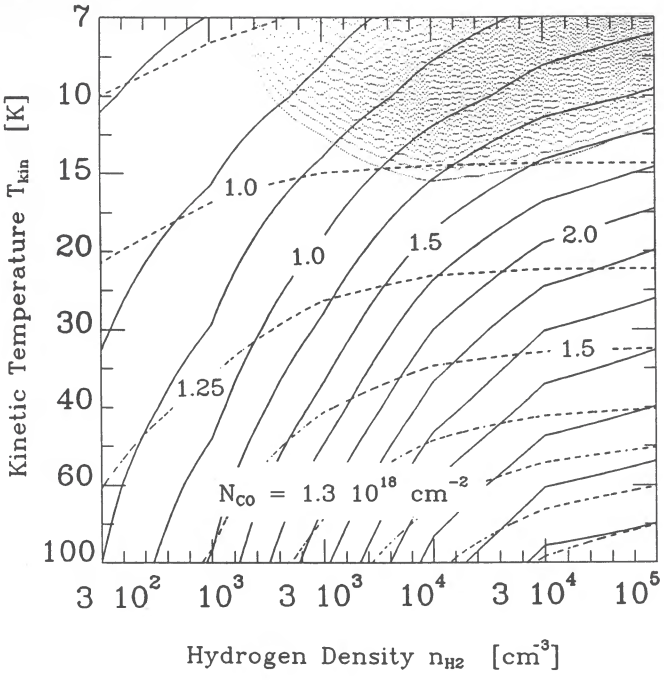

FIG. 8*a*

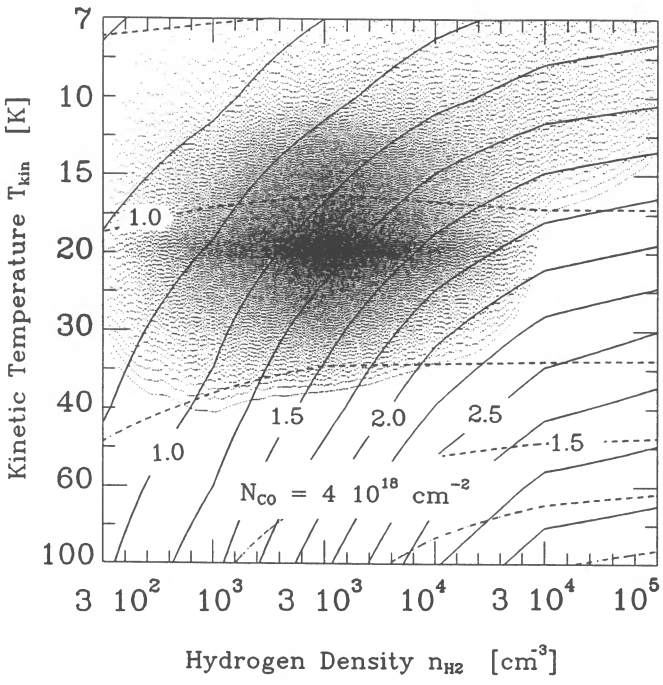

FIG. 8*b*

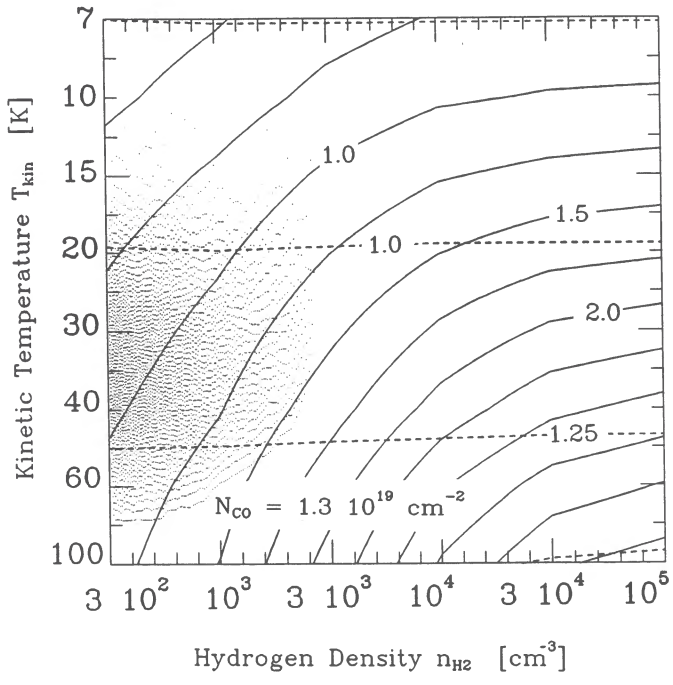

FIG. 8*c*

FIG. 8.—Constraints on the model parameters for the center of IC 342, based on data in Table 4. For line-averaged ^{12}CO column densities N_{CO} of 1.3×10^{18}, 4×10^{18}, and 1.3×10^{19} cm^{-2}, two line ratios are plotted vs. molecular hydrogen density, n_{H_2}, and kinetic temperature, T_{kin}. Broken contours are the $^{12}CO(2 \rightarrow 1)/(1 \rightarrow 0)$ ratio, continuous contours the $^{13}CO(2 \rightarrow 1)/(1 \rightarrow 0)$ ratio. Gray shading is proportional to exp $(-\chi^2)$, χ^2 being calculated from the predicted and measured ratios and intensities and their errors. For solar isotope abundances, the most probable values are $N_{CO} = 4 \times 10^{18}$ cm^{-2}, $n_{H_2} = 3 \times 10^3$ cm^{-3}, and $T_{kin} \geq 20$ K.

and using a dust emissivity at a 100 μm with

$$\frac{a\rho}{Q_{100\,\mu m}} = 0.04 \text{ g cm}^{-2}\,, \tag{6}$$

we find

$$M_{dust} = 4.5 D^2 S_{100\,\mu m}[\exp(144/T_{dust}) - 1]\,, \tag{7}$$

M_{dust} being the dust mass in $M_\odot$, T_{dust} the dust temperature in K, $S(\nu)$ the flux density in Jy, $B(\nu, T_{dust})$ the Planck function, and D the distance to the source in Mpc. Using $S_{100\,\mu m} = 140$ Jy $\pm$ 20% in a 60″ beam (Becklin *et al.* 1980), we calculate $M_{dust} = 3.8 \times 10^5\ M_\odot$. With an assumed gas to dust ratio of 100, this results in a 5–6 times smaller gas mass as implied for the bulk of the molecular gas from the isotopic CO data in the same area (see § IV*b*).

ii) *Cosmic Rays*

As noted by many authors (e.g., Goldsmith and Langer 1978; de Jong, Dalgarno, and Boland 1980) a cosmic-ray ionization rate $\sim 5 \times 10^{-17}$ s^{-1} suffices to heat the gas in dense, molecular clouds to ~ 10 K. It thus seems possible that the gas N and S of the nucleus of IC 342 is heated by cosmic rays and cooled via CO rotational line emission.

For the higher temperatures in the nuclear region, we estimate the CO cooling by comparing the integrated rotational line intensities of the first nine transitions predicted by the model of § IV*a*. For an H_2 density of 3×10^3 cm^{-3}, a CO column density of 4×10^{18} cm^{-2}, and kinetic temperature of >20 K, we find that the cosmic-ray ionization rate must be $\geq 10^{-15}$ s^{-1} to provide sufficient heating. A greatly enhanced cosmic-ray rate (factor of 20 compared to the "standard" rate) might be due to the high star formation in the molecular bar. If the nonthermal radio flux densities are proportional to the cosmic ray density (in uniform magnetic fields with uniform pitch angle distribution), then the radio flux densities in the nuclear region should be 20 times higher than in the disk as

TABLE 6

COMPARISON OF THE CENTRAL 1 KILOPARSEC REGION OF M82, IC 342, AND THE GALAXY

Quantity	M82	IC 342	Galaxy
L_{FIR} ($L_\odot$)	4×10^{10} [a]	4×10^{9} [h]	5×10^{8} [l]
Volume emissivity $\epsilon_{FIR} \sim \epsilon_{uv}$ (ergs cm^{-3})	6×10^{-10} [b]	6×10^{-11} [b]	6×10^{-12}–6×10^{-11} [b]
Pressure of atomic gas (K cm^{-3})	10^6–10^7 [b]	6×10^{5} [i]	3×10^{4} [b]
L_{IR}/M_{H_2} ($L_\odot/M_\odot$)	100–500	20	1–10
T_{kin} derived for molecular gas (K)	≥ 40 [c,d]	≥ 20 [i]	≥ 20 [m]
Total stellar mass ($M_\odot$)	5×10^{8}–10^{9} [e]	10^{9} [j]	10^{10} [n]
H_2 mass ($M_\odot$)	8×10^{7}–4×10^{8} [d,f,g]	2×10^{8} [i,k]	5×10^{7}–4×10^{8} [o,p]

[a] Telesco and Harper 1980.
[b] Lugten *et al.* 1986.
[c] Knapp *et al.* 1980.
[d] Young and Scoville 1984.
[e] Rieke *et al.* 1980.
[f] Jaffe, Becklin, and Hildebrand 1984.
[g] Sutton, Masson, and Phillips 1983.
[h] Becklin *et al.* 1980.
[i] This paper.
[j] Young and Scoville 1982.
[k] Lo *et al.* 1984.
[l] Mezger 1984.
[m] Dickman 1975.
[n] Oort 1977.
[o] Blitz *et al.* 1985.
[p] Sanders, Solomon, and Scoville 1984.

well. The interferometric radio continuum data (Becklin *et al.* 1980; Turner and Ho 1983) show an increase in flux density at the central position over a region which matches our beam sizes. Comparing with single-dish data (Gräve and Beck 1987) and correcting for the thermal flux in the nucleus (Turner and Ho 1983), we find the ratio of 5 GHz nonthermal flux density (nucleus:disk) to be only 4:1, so that cosmic-ray heating is not likely to be the only mechanism responsible for heating the molecular gas.

iii) *UV Field*

Both the far-infrared emission and the extended nonthermal radio emission suggest enhanced star formation in the nuclear region. An increased star formation rate will result in an increased number of OB stars and hence in a more intense UV field at the nucleus. This will result in heating of the surfaces of molecular clouds up to temperatures of a few hundred degrees by means of photoelectric heating and heating through far-UV pumping of H_2 (Tielens and Hollenbach 1985; Sternberg and Dalgarno 1989). This in return results in strong far-infrared cooling lines as reported by Crawford *et al.* (1985) and can also give rise to optically thin emission from hot CO in the photodissociated cloud surfaces.

d) Comparison with Other Sources

In Table 6 we compare physical parameters of M82, IC 342, and the Galaxy. The three galaxies have similar stellar and molecular masses, but they differ by an order of magnitude in far-infrared luminosity, UV energy density, and atomic gas pressure. Consequently their ratios of far-infrared luminosity to H_2 mass, which measure the efficiency of star formation, also differ by an order of magnitude, with IC 342 being intermediate between our Galaxy and M82. The list in Table 6 presents evidence that the character of the interstellar media in galaxies varies substantially with the galaxy's rate of star formation.

V. CONCLUSIONS

1. The structure at the center of IC 342 is concistent with a rotating molecular bar $30'' \times \leq 13''$ in size, elongated NS. There is also evidence for low-level extended emission over $\geq 90''$ at the same position angle as the dust lanes.

2. Observations of the two lower rotational transitions of CO isotopes show that the molecular excitation in the nuclear region of IC 342 varies with position. If all isotopic CO line emission originates from the same molecular material, then the gas is warm ($T_{kin} \geq 20$ K) at the center, while ~ 500 pc N and S of the nucleus the molecular gas is cold (T_{kin} between 10 and 20 K), and along a ridge ~ 500 pc E of the center the kinetic temperature is >40 K.

3. In the bulk of the molecular clouds of IC 342, H_2 volume densities range between 10^3 and 10^4 cm^{-3}. Our model calculations result in conversion factors between the H_2 column density and the $^{12}CO(1 \rightarrow 0)$ line intensity close to the value of 3 to 4×10^{20} cm^{-2}/K km s^{-1} derived for molecular clouds in the Galaxy.

4. The molecular mass in the central two kpc of IC 342 is $\sim 2 \times 10^8$ $M_\odot$. The neutral interstellar medium of IC 342 exhibits properties intermediate between M82 and our Galaxy.

We are grateful to the staff of the IRAM 30 m telescope and the Kuiper Airborne Observatory for their excellent support of these observations. We thank G. Stacey and J. Stutzki for helpful discussions, and B. Wall for communicating his $J = 3 \rightarrow 2$ data prior to publication. M. K. Crawford and J. B. Lugten helped take the far-infrared data on the Kuiper Airborne Observatory.

Note added in manuscript.—M. L. McCall (*A.J.*, **97**, 1341 [1989]) indicates that the distance to IC 342 may have to be revised to 1.8 Mpc. In this case, linear sizes and masses have to be scaled correspondingly.

REFERENCES

Becklin, E. E., Gatley, I., Matthews, K., Neugebauer, G., Sellgren, K., Werner, M. W., and Wynn-Williams, C. G. 1980, *Ap. J.*, **236**, 441.
Blitz, L., Bloemen, J. B. G. M., Hermsen, W., and Bania, T. M. 1985, *Astr. Ap.*, **143**, 267.
Blundell, R., Carter, M., and Gundlach, K. H. 1988, *Internat. J. Infrared Millimeter Waves.*, **9**, 361.
Blundell, R., Gundlach, K. H., Blum, E. J., Ibrügger, J., and Hein, H. 1985, in *Int. Symposium on Millimeter and Submillimeter Radio Astronomy, URSI*, Granada, p. 117.
Boreiko, R., Betz, A. L., and Zmuidizinas, J. 1988, *Ap. J. (Letters)*, **325**, L47.
Crawford, M. K., Genzel, R., Townes, C. H., and Watson, D. M. 1985, *Ap. J.*, **291**, 755.
de Jong, T., Dalgarno, A., and Boland, W. 1980, *Astr. Ap.*, **91**, 68.
Dickman, R. L. 1975, *Ap. J.*, **202**, 50.
Flower, D. R., and Launay, J. M. 1985, *M.N.R.A.S.*, **214**, 271.
Genzel, R., and Stacey, G. J. 1985, *Mitt. Astr. Ges.*, **63**, 215.
Genzel, R., Stacey, G. J., Harris, A. I., Towns, C. H., Geis, N., Graf, U. U., Poglitsch, A., and Stutzki, J. 1989, *Ap. J.*, submitted.
Genzel, R., Watson, D. M., Crawford, M. K., and Townes, C. H. 1985, *Ap. J.*, **297**, 766.

Goldsmith, P. F., and Langer, W. D. 1978, *Ap. J.*, **222**, 881.
Gräve, R., and Beck, R. 1988, *Astr. Ap.*, **192**, 66.
Huntley, J. M. 1978, *Ap. J. (Letters)*, **225**, L161.
Hayashi, M., Handa, T., Sofue, Y., Nakai, N., Hasegawa, T., Lord, S., and Young, J. 1986, in *IAU Symposium 115, Star Forming Regions*, ed. M. Peimbert and J. Jugaku (Dordrecht: Reidel), p. 631.
Hildebrand, R. H. 1983, *Quart. J.R.A.S.*, **24**, 267.
Ho, P. T. P., and Martin, R. N. 1986, *Astr. Ap.*, **308**, L7.
Ho, P. T. P., Turner, J. L., and Martin, R. N. 1987, *Astr. Ap.*, **332**, L67.
Jaffe, D. T., Becklin, E. E., and Hildebrand, R. H. 1984, *Ap. J. (Letters)*, **285**, L31.
Jura, M. 1978, in *Protostars and Planets*, ed. J. Gehrels (Tucson: University of Arizona Press), p. 165.
Knapp, G. R., Phillips, T. G., Huggins, P. J., Leighton, R. B., and Wannier, P. G. 1980, *Ap. J.*, **240**, 60.
Kulkarni, S. R., and Heiles, C. H. 1988, in *Galactic and Extragalactic Radio Astronomy*, ed. K. I. Kellermann and G. L. Verschuur (Berlin: Springer), p. 95.
Kutner, M. L., and Ulich, B. L. 1981, *Ap. J.*, **250**, 341.
Lo, K. Y., *et al.* 1984, *Ap. J. (Letters)*, **282**, L59.
Lugten, J. B. 1987, Ph.D. thesis, University of California, Berkeley.
Lugten, J. B., Genzel, R., Crawford, M. K., and Townes, C. H. 1986, *Ap. J.*, **306**, 691.
Martin, H. M., Sanders, D. B., and Hills, R. E. 1984, *M.N.R.A.S.*, **208**, 35.
McKee, C. F., Storey, J. W. V., Watson, D. M., and Green, S. 1982, *Ap. J.*, **259**, 647.
Mezger, P. G. 1984, in *Galactic and Extragalactic Infrared Spectroscopy*, ed. M. F. Kessler and J. P. Phillips (Dordrecht: Reidel), p. 423.
Morris, M., and Lo, K. Y. 1978, *Ap. J.*, **223**, 803.
Oort, J. H. 1977, *Ann. Rev. Astr. Ap.*, **15**, 295.
Rickard, L. J, and Palmer, P. 1981, *Astr. Ap.*, **102**, L13.
Rickard, L. J, Palmer, P., Morris, M., Zuckermann, B., and Turner, B. E. 1975, *Ap. J. (Letters)*, **199**, L75.
Rieke, G. H., Lebofsky, M. J., Thompson, R. I., Low, F. J., and Tokunaga, A. T. 1980, *Ap. J.*, **238**, 24.
Rogstad, D. H., and Shostak, G. S. 1973, *Astr. Ap.*, **22**, 111.
Sanders, D. B., Solomon, P. M., and Scoville, N. Z. 1984, *Ap. J.*, **276**, 182.
Schinke, R., Engel, V., Buck, U., Meyer, H., and Diercksen, G. H. F. 1985, *Ap. J.*, **299**, 939.
Shaya, E. J., and Federman, S. R. 1987, *Ap. J.*, **319**, 76.
Solomon, P. M., Rivolo, A. R., Barrett, J., and Yahil, A. 1987, *Ap. J.*, **319**, 730.
Stacey, G. J. 1985, Ph.D. thesis, Cornell University.
Stacey, G. J., Genzel, R., Lugten, J. B., and Townes, C. H. 1990, in preparation.
Stacey, G. J., Viscuso, P. J., Fuller, C. E., and Kurtz, N. T. 1985, *Ap. J.*, **289**, 803.
Sternberg, A., and Dalgarno, A. 1989, *Ap. J.*, **338**, 197.
Storey, J. W. V., Watson, D. M., and Townes, C. H. 1980, *Internat. J. Infrared Millimeter Waves*, **1**, 15.
Sutton, E. C., Masson, C. R., and Phillips, T. G. 1983, *Ap. J. (Letters)*, **275**, L49.
Telesco, C. M., and Harper, D. A. 1980, *Ap. J.*, **235**, 392.
Tielens, A. G. G. M., and Hollenbach, D. 1985, *Ap. J.*, **291**, 722.
Turner, J. L., and Ho, P. T. P. 1983, *Ap. J. (Letters)*, **268**, L79.
Ulich, B. L., and Haas, R. W. 1976, *Ap. J. Suppl.*, **30**, 247.
Watson, D. M. 1982, Ph.D. thesis, University of California, Berkeley.
Watson, D. M., *et al.* 1984, in *Galactic and Extragalactic Infrared Spectroscopy*, ed. M. F. Kessler and J. P. Phillips (Dordrecht: Reidel), p. 195.
Young, J. S., and Scoville, N. 1982, *Ap. J.*, **258**, 467.
———. 1984, *Ap. J.*, **287**, 153.

A. Eckart, R. Genzel, A. I. Harris, and W. Wild: Max-Planck-Institut für Physik und Astrophysik, Institut für Extraterrestrische Physik, 8046 Garching, Federal Republic of Germany

D. Downes: Institut de Radio Astronomie Millimétrique, Domaine Universitaire, 38406 St.-Martin-D'Héres, France

D. T. Jaffe: Astronomy Department, University of Texas, R. L. Moore Hall, Austin, TX 78712